Detection of significant antiviral drug effects on COVID-19 with reasonable sample sizes in randomized controlled trials: a modeling study combined with clinical data

Authors:

Shoya Iwanami[1,†], Keisuke Ejima[2,†*], Kwang Su Kim[1], Koji Noshita[1], Yasuhisa Fujita[1], Taiga Miyazaki[3], Shigeru Kohno[4], Yoshitsugu Miyazaki[5], Shimpei Morimoto[6], Shinji Nakaoka[7], Yoshiki Koizumi[8], Yusuke Asai[9], Kazuyuki Aihara[10], Koichi Watashi[11,12,13,14], Robin N. Thompson[15,16], Kenji Shibuya[17], Katsuhito Fujiu[18,19], Alan S. Perelson[20,21,‡], Shingo Iwami[1,12, 22,23,24, ‡*], Takaji Wakita[11]

Affiliations:

[1] Department of Biology, Faculty of Sciences, Kyushu University, Fukuoka, Japan 8190395.

[2] Department of Epidemiology and Biostatistics, Indiana University School of Public Health-Bloomington, IN, USA 47405.

[3] Department of Infectious Diseases, Nagasaki University Graduate School of Biomedical Sciences, Nagasaki, Japan 8528501.

[4] Nagasaki University, Nagasaki, Japan 8528521.

20 [5] Department of chemotherapy & mycoses, and Leprosy Research Ctr., National
21 Institute of Infectious Diseases, Tokyo, Japan 3320012.

22 [6] Institute of Biomedical Sciences, Nagasaki University, Japan 8528501.

23 [7] Faculty of Advanced Life Science, Hokkaido University, Sapporo, Japan 0600808.

24 [8] National Center for Global Health and Medicine, Tokyo, Japan 1628655.

25 [9] Disease Control and Prevention Center, National Center for Global Health and
26 Medicine, Tokyo, Japan 1628655.

27 [10] International Research Center for Neurointelligence, The University of Tokyo
28 Institutes for Advanced Study, The University of Tokyo, Tokyo, Japan.

29 [11] Department of Virology II, National Institute of Infectious Diseases, Tokyo, Japan
30 1628640.

31 [12] MIRAI, JST, Saitama, Japan 3320012.

32 [13] Department of Applied Biological Science, Tokyo University of Science, Noda, Japan
33 2788510.

34 [14] Institute for Frontier Life and Medical Sciences, Kyoto University, Kyoto, Japan
35 6068507.

36 [15] Mathematics Institute, University of Warwick, Coventry CV4 7AL, UK.

37 [16] Zeeman Institute for Systems Biology and Infectious Disease Epidemiology
38 Research, University of Warwick, Coventry CV4 7AL, UK.

39 [17] Institute for Population Health, King's College London, London SE1 1UL, UK.

[18] Department of Cardiovascular Medicine, Graduate School of Medicine, The University of Tokyo, Tokyo, Japan 1138655.

[19] Department of Advanced Cardiology, Graduate School of Medicine, The University of Tokyo, Tokyo, Japan 1138655.

[20] Theoretical Biology and Biophysics Group, Los Alamos National Laboratory, Los Alamos, NM 87545, USA.

[21] New Mexico Consortium, Los Alamos, NM 87544, USA

[22] Institute for the Advanced Study of Human Biology (ASHBi), Kyoto University, Kyoto 6068501, Japan.

[23] NEXT-Ganken Program, Japanese Foundation for Cancer Research (JFCR), Tokyo 1358550, Japan.

[24] Science Groove Inc., Fukuoka 8100041, Japan.

*Correspondence to kejima@iu.edu (KE) and iwamishingo@gmail.com (SI)

†, ‡ These authors contributed equally to this study.

Abstract

Background

Development of an effective antiviral drug for COVID-19 is a global health priority. Although several candidate drugs have been identified through *in vitro* and *in vivo* models, consistent and compelling evidence from clinical studies is limited. The lack of evidence from clinical trials may stem in part from the imperfect design of the trials, which may fail to incorporate two critical factors: 1) heterogeneity in virus dynamics among patients and 2) timing of treatment initiation. However, it remains unclear how SARS-CoV-2 virus dynamic differs among patients and how clinical studies of antiviral drugs for COVID-19 have to be designed.

Methods and Findings

To help understand the reasons behind inconsistent clinical trial findings, we performed a modelling study. We first analyzed longitudinal viral load data for SARS-CoV-2 without antiviral treatment by use of a within-host virus dynamics model. The fitted viral load was categorized into three different groups by a clustering approach. Comparison of the estimated parameters showed that the three distinct groups were characterized by different virus decay rates (p-value<0.001). The decay rates were 1.17 d^{-1} (95% CI: 1.06 to 1.27 d^{-1}), 0.777 d^{-1} (0.716 to 0.838 d^{-1}), and 0.450 d^{-1} (0.378 to 0.522 d^{-1}) for the three groups, respectively. Such heterogeneity in virus dynamics could be a confounding variable if it is associated with treatment allocation in compassionate use programs (i.e., observational studies).

Subsequently, we mimicked randomized controlled trials of antivirals by simulation. An antiviral effect causing a 95% to 99% reduction in viral replication was added to the model. To be realistic, we assumed that randomization and treatment are initiated with some time lag after symptom onset. Using the duration of virus shedding as an outcome, the sample size to detect a statistically significant mean difference between the treatment and placebo groups (1:1 allocation) was 13,603 and 11,670 (when the antiviral effect was 95% and 99%, respectively) per group if all patients are enrolled regardless of timing of randomization. The sample size was reduced to 584 and 458 (when the antiviral effect was 95% and 99%, respectively) if only patients who are treated within 1 day of symptom onset are enrolled. We confirmed the sample size was similarly reduced when using cumulative viral load in log scale as an outcome.

We used a conventional virus dynamics model which does not fully reflect the detailed physiological processes of virus replication of SARS-CoV-2 and excluded viral load data under treatment to evaluate our model. Further investigation should find factors not incorporated in the model, which would yield more reliable sample size calculation.

Conclusions

In this study, we found large heterogeneity in virus dynamics among infected individuals, characterized by different virus decay rates, and the time of treatment initiation as important factors behind the inconsistent or null findings of clinical studies of the antiviral effect of treatments for SARS-CoV-2 infection. In clinical trials that have failed to identify effective antiviral drugs against SARS-CoV-2, there may be at least two reasons behind this: 1) randomization is not performed (i.e., observational studies), and

100 2) randomization and treatment initiation are delayed. For a statistically significant effect
101 of antiviral drugs on COVID-19 to be observed a study's design should consider these
102 two factors.

Author Summary

■ Why was this study done?

- Most clinical studies of antiviral drugs for SARS-CoV-2 have failed to observe a statistically significant effect.
- The confounding factors leading to the failure of antiviral drug clinical trials and the suitable design for successful clinical trials of antiviral drugs against SARS-CoV-2 are unknown.

■ What did the researchers do and find?

- SARS-CoV-2 virus dynamics was quantified by fitting a virus dynamic model to longitudinal viral load data.
- Cluster analysis of the fitted viral loads revealed three distinct groups characterized by different virus decay rates, which could be a confounding factor in observational studies.
- Simulation mimicking randomized controlled trials demonstrated that sample size would be unreasonably large (>11,000 per group) if the timing of treatment initiation is not considered. The sample size is significantly reduced by including only patients enrolled early after symptom onset.

■ What do these findings mean?

- Randomized controlled trials for antiviral drugs should recruit patients as early as possible after symptom onset or set inclusion criteria based on the time since symptom onset to observe statistically significant results.

124 • More precise models reflecting the features of SARS-CoV-2 infection may provide
125 more reliable sample size estimates.
126

127 # Introduction

128 Development of an effective antiviral drug for COVID-19 is a global health
129 priority. Along with the development of new antiviral drugs, repurposing of existing drugs
130 for COVID-19 treatment has accelerated [1]. Some antiviral drugs have shown high
131 efficacy against severe acute respiratory syndrome coronavirus 2 (SARS-CoV-2) in both
132 *in vitro* and *in vivo* models [2, 3]. A number of clinical studies such as compassionate
133 use programs and clinical trials have been conducted or are underway to test the
134 efficacy of FDA-approved drugs, such as lopinavir and ritonavir, chloroquine, favipiravir,
135 and remdesivir [4-9]. Different drugs have different modes of action, but the majority of
136 the candidate antiviral drugs for SARS-CoV-2 are expected to block virus replication.
137 Lopinavir/ritonavir are HIV protease inhibitors, and remdesivir was originally developed
138 to mitigate the replication of hepatitis C viruses (and considered potentially useful for
139 Ebola virus). Other nucleoside analogues [10, 11] are also candidates for mitigating
140 SARS-CoV-2 replication within the host.

141 However, the results from those clinical studies were often nonsignificant and
142 sometimes inconsistent. This may be in part attributable to a nonrigorous study design,
143 which masks the true efficacy of antivirals [12]. Clinical trial design usually takes months
144 to formulate the study protocol (i.e., dose of drugs, clinical outcomes to be evaluated,
145 sample size, assessment of safety), and requires collecting preliminary data. However,
146 the urgent need to find effective antiviral treatments for COVID-19 may have led to
147 rushed studies.

148 In compassionate use programs (i.e., observational studies), whether and when
149 antiviral treatment is initiated is determined by health practitioners along with patients

150 and their next of kin. By the very nature of these studies, potential confounders, such as
151 the patients' clinical characteristics and preexisting conditions, influence both treatment-
152 control allocation and clinical outcomes. As a consequence, conclusions from the
153 program could be biased even when all observable confounders are addressed in the
154 analysis [13]. However, such programs are widely used for hypothesis building.
155 Contrary to compassionate use programs, clinical trials, particularly randomized
156 controlled trials, are considered robust against confounder effects and the most reliable
157 study design. **Table S1** summarizes the current major clinical studies for antiviral
158 treatment of SARS-CoV-2. Indeed, the results from these clinical studies have yielded
159 null or inconsistent findings. For example, compassionate use of hydroxychloroquine
160 was reported in many articles, but the findings were not consistent. Gautret et al.
161 reported significant antiviral efficacy [14], whereas Geleris et al. could not replicate the
162 result [15].

163 To help understand the mechanism behind the inconsistent findings, we
164 parametrized the virus dynamics model which we previously developed [16-18] by using
165 longitudinal viral load data extracted from clinical studies and further ran simulations
166 adding antiviral effects to the model. Here, we demonstrate that at least two factors can
167 mask the effects of antiviral drugs in clinical studies for COVID-19: 1) heterogeneity in
168 virus dynamics among patients and 2) late timing of treatment initiation. We also
169 propose a novel approach to the best of our knowledge to calculating the sample size
170 (i.e., the required or minimum sample size needed to infer whether the antiviral drug is
171 effective assuming the drug is truly effective) accounting for within-host virus dynamics.

Methods

Study data

The longitudinal viral load data examined in our study were extracted from the published studies of SARS-CoV-2: Young et al. [19], Zou et al. [20], Kim et al. [21], and Wölfel et al. [22]. For consistency, the viral load data measured from upper respiratory specimens were used. We excluded patients who received antiviral treatment and for whom data were measured on only 1 or 2 days (because one or two data points are not enough to estimate parameters). We converted cycle threshold (Ct) values to viral RNA copy number values, where these quantities are inversely proportional to each other [20]. In total, we use the data from 30 patients. To extract the data from the images in those papers, we used the software datathief III (version 1.5, Bas Tummers, www.datathief.org).

Mathematical model for virus dynamics without and with antiviral treatment

SARS-CoV-2 virus dynamics without antiviral treatment is described by a mathematical model previously proposed in [23-25].

$$\frac{df(t)}{dt} = -\beta f(t)V(t), \tag{1}$$

$$\frac{dV(t)}{dt} = \gamma f(t)V(t) - \delta V(t), \tag{2}$$

where $f(t)$ is the relative fraction of uninfected target cells at time t to those at time 0 and $V(t)$ is the amount of virus at time t, respectively. Both $f(t)$ and $V(t)$ are in linear

192 scale. The parameters β, γ, and δ represent the rate constant for virus infection, the
193 maximum rate constant for viral replication, and the per capita death rate of virus-
194 producing cells, respectively. Note that δ implicitly includes the effects of the immune
195 response in killing infected cells, e.g. by cytotoxic T lymphocytes. All viral load data
196 were fit using a nonlinear mixed-effect modelling approach, which estimates population
197 parameters while accounting for inter-individual variation in virus dynamics (see the next
198 section for detail). The day from symptom onset was used as a time scale (i.e., $t = 0$ at
199 symptom onset).

200 The virus dynamic model under antiviral treatment (which we assume blocks
201 virus replication) initiated at t^* days after symptom onset can be described based on the
202 above model as follows:

203 $$\frac{df(t)}{dt} = -\beta f(t)V(t), \quad (3)$$

204 $$\frac{dV(t)}{dt} = \big(1 - \varepsilon \times H(t)\big)\gamma f(t)V(t) - \delta V(t), \quad (4)$$

205 where $H(t)$ is a Heaviside function indicating off- and on-treatment, defined as $H(t) = 0$
206 if $t < t^*$ (i.e., before treatment initiation); otherwise $H(t) = 1$. ε is the fraction of virus
207 production inhibited by the therapy ($0 < \varepsilon \leq 1$). $\varepsilon = 1$ when the virus replication from the
208 infected cells is totally inhibited (i.e., the antiviral effect is 100%). We evaluated the
209 expected antiviral effect of the treatment on the outcomes (duration of virus shedding
210 and cumulative viral load measured on a log scale) under different inhibition rates (ε)
211 and initiation times (t^*). The effect of drugs that blocking *de novo* infection can be
212 modeled by inhibiting both the $\beta f(t)V(t)$ and $\gamma f(t)V(t)$ terms and a drug promoting
213 cytotoxicity can be modeled by increasing $\delta V(t)$, as we discussed in [24]. Unfortunately,

because sufficient viral load data under antiviral drug therapy are not available yet, the antiviral effect (ε) of drugs in preclinical development and in clinical trials are still unknown. Therefore, we chose to examine hypothetical examples of drugs with 50%, 95%, or 99% efficacy. We used 50% and 99% efficacy to illustrate the difference in viral dynamics between patients with and without treatment (see section "**SARS-CoV-2 virus dynamics and antiviral effect**"), and 95% and 99% efficacy in "**Simulation mimicking a randomized controlled trial for antiviral drugs**". Since clinical trials are performed only for drugs with sufficient efficacy (i.e., there is no reason to test drugs with weak efficacy), we believe this value range is reasonable.

Parameter estimation with the nonlinear mixed-effects model

A nonlinear mixed-effects model was used to fit the viral dynamic model given by equations [Eq1] and [Eq2] to the longitudinal viral load data. The model included both a fixed effect (constant across patients) and a random effect (different between patients) in each parameter. Specifically, the parameter for patient k, ϑ_k $(= \vartheta \times e^{\pi_k})$ is represented as a product of ϑ (a fixed effect) and e^{π_k} (a random effect). π_k follows the normal distribution with mean 0 and standard deviation Ω. Fixed effects and random effects were estimated using the stochastic approximation expectation-maximization algorithm and empirical Bayes' method, respectively. The conditional distribution of the vector of individual parameters was estimated for each patient using the Metropolis-Hastings algorithm and was used to calculate the 95% predictive interval of the viral load curve in **Fig. 1**. The mixed model approach is becoming more common in longitudinal viral load data analysis [18, 26], because it can capture the heterogeneity in

virus dynamics, and parameter estimation is feasible even for those with limited data. Fitting was performed using MONOLIX 2019R2 (www.lixoft.com) [27]. To account for data points under the detection limit (see the red dots in **Fig. S1**), the likelihood function reflected the likelihood that the data are in the censoring interval (0 to the detection limit) given parameter values with a right-truncated Gaussian distribution [28].

Clustering of individual viral load dynamics

As observed in **Fig. 1**, the virus dynamics has huge heterogeneity between patients. For some patients, viral load declines rapidly, but for others, it persists for almost 1 month. It is ideal if the longitudinal viral load data can be directly compared between patients; however, the data collection intervals are not the same between patients, and the data under the detection limit are not quantifiable. Therefore, we used the fitted viral load every day since symptom onset, which is available from the best fit curve, for comparison. The fitted daily viral load values of each patient were rescaled by their maximum values and log-transformed. Then, hierarchical clustering was performed on the rescaled-transformed fitted daily viral load using the linkage function with Ward's method [29] in SciPy [30]. Once multiple clusters are identified, estimated parameter distributions among the clusters were compared by ANOVA to assess the source of the difference in virus dynamics. Pairwise comparison was subsequently performed using Student's *t* test. The p-values of the pairwise Student's *t* test were adjusted by the Bonferroni correction.

259 **Simulation mimicking a randomized controlled trial for antiviral drugs**

260 We mimicked randomized controlled trials using the model including the effects
261 of an antiviral drug. The allocation ratio is assumed as 1:1 (control:treatment). A total of
262 20,000 parameter sets were randomly sampled from the estimated distributions of
263 individual parameters. A longitudinal viral load time series for each individual was
264 created based on their chosen parameter set. Note that for those in the treatment
265 group, the antiviral effect (ε) was assumed to be constant. For sensitivity analysis, we
266 used two different values of ε, 95% and 99%. To obtain a realistic simulation, treatment
267 was initiated following the distribution of time from symptom onset to hospitalization
268 obtained from Bi et al.: *lognorm*(1.23, 0.79) (the mean is 4.64 days) [31], where the
269 treatment was assumed to be initiated immediately after hospitalization. We also used a
270 truncated distribution to mimic the randomized controlled trials including only patients
271 recruited and treated early (within 0.5, 1, 2, 3, and 4 days after symptom onset).

272 We used two quantities as outcome measures: the duration of virus shedding
273 from the onset of symptoms until the time the virus becomes undetectable (T_D), and the
274 log10-transformed cumulative viral load, i.e., the area under the curve (AUC) of viral
275 load ($\log_{10}$(AUC): $\log_{10} \int_0^{T_D} V(s)ds$). Many clinical studies have used the duration of viral
276 shedding as a primary outcome (see **Table S1**) and previous theoretical studies have
277 quantified the AUC. Both of the outcomes we use here are expected to be reduced
278 under effective antiviral treatment.

279 From our simulations we obtained 10,000 outcomes for each group (duration of
280 virus shedding and cumulative viral load). The sample size was computed for different

values of ε using the two-tailed Welch's *t* test with significance level and power as 0.05 and 80%, respectively.

Results

Heterogeneity in SARS-CoV-2 virus dynamics

SARS-CoV-2 viral load data were analyzed using a mathematical model to quantify the heterogeneity in virus dynamics among patients and to examine the source of the heterogeneity. Longitudinal viral load data from 30 patients from different countries were fitted simultaneously using a nonlinear mixed-effects modelling approach. With the estimated parameters for each patient (listed in **Table S2**), viral loads since the time of symptom onset were fully reconstructed even when the viral load was missed or under the detection limit (**Fig.1** and **Fig.2A**). This reconstruction allowed us to quantitatively compare viral load dynamics between patients. The viral loads over time, which were reconstructed based on the mathematical model with the estimated parameters, were analyzed with a clustering approach (**Fig.2B**) and placed into three groups. Patient "China O" was detected as an outlier and was excluded from further analysis.

To understand the source of the difference in virus dynamics between groups, we tested the differences in the estimated parameters (i.e., β, γ, δ and $V(0)$) among the groups. Statistically significant between-group differences were found in the maximum rate constant for viral replication, γ, and in the death rate of virus-producing cells per day, δ (**Fig.S1**). The differences in γ are related to the growth of viral load (a larger γ indicates more rapid growth); however, the difference in γ between groups was sufficiently small that its influence on virus dynamics especially after the viral load peak (or symptom onset) is negligible. The difference in δ manifests in the speed of viral load decay; that is, a small value of δ corresponds to a slow decay in viral load (**Fig.2B**).

306 Thus, we named the three groups as rapid, medium, and slow viral load decay groups
307 (**Fig.3A**). The means of decay rates were 1.17 d^{-1} (95% CI: 1.06 to 1.27 d^{-1}), 0.777 d^{-1}
308 (0.716 to 0.838 d^{-1}), and 0.450 d^{-1} (0.378 to 0.522 d^{-1}) for the three groups, respectively
309 and the minimum and maximum of the decay rate for the three identified groups were
310 0.270 d^{-1} to 0.616 d^{-1} (slow), 0.700 d^{-1} to 0.914 d^{-1} (medium), and 0.993 d^{-1} and 1.30 d^{-1}
311 (rapid). The border value of the decay rate between groups is defined as the mean of
312 the highest value in the lower group and the lowest value in the higher group. Thus, the
313 border value of the slow and medium groups was 0.658 d^{-1} $[(0.616 + 0.700)/2]$, and that
314 of the medium and rapid groups was 0.953 d^{-1} $[= (0.914 + 0.993)/2]$.

315

316 **SARS-CoV-2 virus dynamics and antiviral effect**

317 Using our mathematical model and the estimated parameter distribution for each
318 patient (**Table S3**), we conducted *in silico* experiments to determine the possible
319 therapeutic response, measured in terms of virus dynamics, of drug treatments blocking
320 virus replication. Clinical outcomes are known to be related to the timing of initiation of
321 antiviral treatment in general and especially for influenza [24, 32-35], and the antiviral
322 effects of a treatment are dependent on dose and the patients' immune system [36, 37].
323 Thus, we studied several different scenarios in which we varied the time of treatment
324 initiation (0.5 or 5 days from symptom onset, which were before and generally after the
325 estimated peak viral load in our dataset) and the inhibition rate (99% or 50%). We
326 resampled a total of 1,000 parameter sets from the estimated parameter distributions for
327 this simulation and separated the individuals according to the value of the viral load
328 decay rate (i.e., rapid, $\delta > 0.953$ d^{-1}; medium, 0.658 $d^{-1} \leq \delta \leq 0.953$ d^{-1}, or slow, $\delta <$

329 0.658 d^{-1}). We found that early initiation of antiviral treatment with a high inhibition rate
330 (i.e., 99%) immediately reduced the viral load after initiation (**Fig.2B** and **Fig.S3**).
331 However, if the inhibition rate was low (i.e., 50%), the viral load kept increasing, and the
332 viral load decay rate after the peak was slower or equivalent to that without treatment.
333 This was because viral replication was not efficiently inhibited and thus it continued
334 albeit with a lower rate even after treatment initiation and continued long after the peak.
335 In contrast, virus dynamics was not much influenced if treatment was initiated after the
336 peak regardless of the inhibition rate or the patient type (**Fig.3B** and **Fig.S2**), because
337 the number of uninfected targeted cells remaining at this stage of infection is limited. It
338 is intriguing that a weak antiviral effect was observed for patients with rapid decay even
339 when the treatment was initiated after the peak. Because the virus is removed rapidly
340 during the course of infection for patients with rapid decay, more uninfected cells remain
341 compared with the other groups. Therefore, antiviral drugs can mitigate replication of
342 the virus even when treatment is initiated after the peak to some extent. Note that these
343 findings are not unique to SARS-CoV-2; similar findings for virus dynamics and antiviral
344 effects have been suggested in other infectious diseases [17, 38].

345

346 **Observational studies for antiviral drugs cannot yield significant results owing to**
347 **heterogeneity in virus dynamics**

348 We explored why compassionate use programs do not yield significant findings
349 when using the duration of virus shedding as an outcome. Duration of virus shedding is
350 one of the most frequently used outcomes for assessing antiviral treatment for SARS-
351 CoV-2 infection (**Table S1**) [4, 5, 7, 38]. The distribution of the duration of virus

352 shedding without treatment in the different virus decay groups is shown in **Fig.4A** and
353 **Fig.S3A**. As can be expected from the difference in viral load dynamics, the duration of
354 virus shedding without treatment is longer in the group with slow viral load decay: the
355 averages in the groups with medium, rapid, and slow decay were 12.3 (SD: 1.06), 8.86
356 (SD: 1.40), and 22.5 (SD: 8.15) days, respectively. As a sensitivity analysis we also
357 computed and compared the cumulative viral load (area under the curve; AUC). We
358 confirmed the same trend in the cumulative viral load in log scale (**Fig.S3B** and
359 **Fig.S4A**). We further compared the outcomes under antiviral treatment (inhibition rate
360 was set as 50% and 99%). Regardless of viral decay rate group, we consistently
361 observed that both outcomes were improved by early treatment initiation (day 0.5) but
362 not by late treatment initiation (day 5), as illustrated in **Fig.4B** and **Fig.S4B**.

363 If a patient possesses strong viral defenses, including immune-mediated
364 defenses, the virus-producing cells are removed quickly, which corresponds to a shorter
365 duration of virus production and rapid viral load decay. Indeed, the duration of virus
366 shedding in respiratory samples has been associated with disease severity [39] and
367 differs between symptomatic and asymptomatic cases [40]. Taken together, these
368 findings suggest that both treatment allocation and clinical outcomes in compassionate
369 use programs are associated with severity; thus, severity is a potential confounding
370 variable. Further, there may be other confounding variables in the assessment of
371 treatment efficacy in compassionate use programs; however, controlling all of them in
372 the analysis is not possible. For example, heterogeneous immune responses, which are
373 partially represented by the death rate of infected cells in the model, can confound the

374 inference. However, quantifying the immune response is difficult. We need to be careful
375 when interpreting the results from compassionate use programs.

376

377 **Randomized controlled trials need to enroll patients early after symptom onset to**
378 **observe significant antiviral effects**

379 In contrast to observational studies, randomized controlled trials may not be
380 influenced by confounding variables and could provide valid inference. However, clinical
381 trials for COVID-19 should consider the timing of treatment initiation in the design (i.e.,
382 inclusion-exclusion criteria), because differences in outcomes are unlikely to be
383 observed under late treatment initiation as we demonstrated in the previous section
384 (**Fig.4B and Fig.S4B**).

385 We computed the sample size needed to observe a statistically significant
386 difference in outcomes with 80% power and a significance level of 0.05 assuming
387 patients are randomly assigned and treated (with antiviral or placebo) immediately after
388 hospitalization with different antiviral effect (95% and 99%) (**Fig.5A**) and with different
389 inclusion and exclusion criteria for the timing of enrollment. We primarily used the
390 duration of virus shedding as an outcome, but the results are qualitatively consistent for
391 cumulative viral load as an outcome. The sample size is strongly dependent on the
392 criterion of the timing of enrollment; that is, the sample size can be reduced if patients
393 are enrolled early after symptom onset (**Table S4**). The distribution of duration of virus
394 shedding under the different criteria is shown in **Fig.5BC**. If patients are enrolled
395 regardless of the time of treatment initiation, the sample sizes are 13,603 and 11,670
396 per group when the inhibition rate is 95% and 99%, respectively, which is much larger

397 than the empirical sample size of the randomized controlled trials of antivirals for SARS-
398 CoV-2 (**Table S1**). This large sample size is needed given that the treatment is initiated
399 4.6 days after onset of symptoms on average, which is after the viral load peak. If we
400 enroll only the patients treated within 1 day of the onset of symptoms, the sample size is
401 reduced to 584 and 458 per group when inhibition rate is 95% and 99%, respectively.
402 Note that antiviral drugs with a weaker inhibition rate will require larger sample sizes.
403 The trend was similar when cumulative viral load in log scale was used as an outcome
404 (**Table S4** and **Fig.S4CD**).

405

406 **Timing of randomization of clinical studies of antiviral drugs for SARS-CoV-2**

407 To validate our findings from a practical perspective, we checked the clinical
408 trials investigating antiviral efficacy registered in ClinicalTrials.gov. As of 22 May 2020,
409 we identified 176 clinical trials with the search terms “antiviral” and “COVID.” Among
410 them, 46 studies did not investigate the efficacy of antiviral drugs (the effect of anti-
411 inflammatory drugs were investigated, for example), and 20 studies did not directly
412 investigate the efficacy of antivirals (such as vaccine studies, safety studies). Among
413 the remaining 110 studies investigating antiviral effect, including remdesivir, chloroquine,
414 and lopinavir/ritonavir, only 17 studies (15%) explicitly stated the time from symptom
415 onset in the inclusion or exclusion criteria. The average time from symptom onset to
416 randomization was 7.2 days, which our findings suggest is too late to observe a
417 statistically significant antiviral effect with a reasonable sample size.

418 # Discussion

419 We explored the mechanism behind the inconsistent or null findings of clinical
420 studies of the antiviral effect of treatments for SARS-CoV-2 infection. By fitting a
421 conventional virus dynamics model to the longitudinal viral load data from patients with
422 COVID-19 (without antiviral treatment), we found that there is large heterogeneity in
423 virus dynamics, as characterized by different virus decay rates. Such heterogeneity in
424 virus dynamics could be a confounding factor in observational studies. Subsequently, a
425 set of randomized controlled trials were mimicked by using a version of the model with
426 an antiviral effect. We assumed that therapy was initiated as soon as a participant was
427 hospitalized with COVID-19 symptoms. We used a reported distribution of time delays
428 from symptom onset to hospitalization in China to make the simulation more realistic.
429 When we included all patients in the trial regardless of the timing of randomization and
430 treatment initiation (1:1 allocation for treatment:placebo), we found that more than
431 11,000 patients per group would need to be recruited. By including only patients
432 hospitalized within 1 day since symptom onset, the sample size is reduced to about 450
433 per group. Thus, we conclude that clinical trials should consider the time of treatment
434 initiation in the study design.

435 In randomized controlled trials, the calculation of sample size has been
436 performed directly by assuming specific distributions for outcomes with a prespecified
437 effect size [41]. However, as we demonstrated, the antiviral effect is determined not only
438 by dose and type of drug, but also by the timing of treatment initiation and the
439 parameters that govern the virus dynamics. Further, the association between treatment
440 initiation and the outcome (length of viral shedding) is nonlinear; thus, our mathematical

441 model-based approach can provide a more reliable sample size than a conventional
442 effect size-based approach.

443 We used measurements related to viral load as outcomes in this study rather
444 than mortality. Mortality is an important and ultimate clinical outcome at both the
445 individual and the population level. However, that does not undermine the value of
446 outcomes related to viral load (such as the duration of virus shedding), which have a
447 different interpretation than clinical outcome. One thing that can be captured by viral
448 load but not by clinical outcome is potential transmissibility. From a clinical viewpoint,
449 each drug has its purpose of use. For example, immunosuppressive agents (e.g.,
450 dexamethasone) are expected to reduce clinical symptoms and mortality. Meanwhile,
451 the efficacy of antiviral drugs should be evaluated primarily by using viral load. In
452 addition, the major objective of therapy depends on the severity of disease. Lifesaving is
453 the most important for patients with severe illness. For mild cases, physicians attempt to
454 prevent the condition and spread of infection from getting worse by using drugs with few
455 adverse effects. A primary endpoint should be determined on the basis of the objectives
456 and goals of clinical trials. As most COVID-19 patients have mild to moderate disease,
457 the duration of viral shedding would be more appropriate than mortality as a primary
458 outcome. Indeed, many studies have used the duration of viral shedding as an outcome
459 (**Table S1**).

460 Regarding the association between viral load and clinical outcomes such as
461 mortality and clinical scores, it has been observed in a number of studies that a high
462 viral load at diagnosis is associated with severe clinical outcomes [39, 42, 43] and
463 increased risk of mortality [44]. The data we used in this study do not contain clinical

464 outcomes, thus we cannot correlate our results with clinical outcomes. However,
465 assuming that the viral load at diagnosis is close to the viral load at symptom onset,
466 $V(0)$, we did not find a significant difference in $V(0)$ between groups. The groups we
467 identified were characterized by a difference in the death rate of virus-producing cells
468 which was reflected in the virus decay rate. Combining our findings with those from the
469 literature, disease severity might not be associated with a difference in overall viral
470 dynamics. For prognosis purposes, we need to better understand when and which
471 biomarkers including the viral load differentiate between severe and non-severe cases.

472 The strength and uniqueness of our approach is that we accounted for virus
473 dynamics in the assessment of antiviral effects and sample size calculations. As far as
474 we know, considering the timing of treatment initiation in a conventional approach to
475 sample size calculation is challenging, especially because the outcome is nonlinearly
476 dependent on the timing of treatment initiation. Even if it is technically possible, the data
477 including the timing of treatment initiation would be limited or small. We used clinical
478 data from SARS-CoV-2-infected patients for the simulation. Thus, our numerical results
479 are realistic and directly interpretable for drug development for SARS-CoV-2. In other
480 words, our approach is flexible and can be applied to other antiviral drugs for other
481 diseases by replacing the dataset.

482 There are several limitations in our approach. First, our within-host virus
483 dynamics model does not fully reflect the detailed physiological processes of virus
484 replication of SARS-CoV-2. For example, our mathematical model assumed target cells
485 are a homogeneous population (i.e., single-target cell compartment). The susceptibility
486 of target cells for SARS-CoV-2 infection is, however, dependent on expression levels of

its receptor, angiotensin converting enzyme 2 (ACE2) [45], and therefore susceptibility to infection might be heterogeneous (i.e., multi-target cell compartments) even in the same organ. However, the virus dynamics of our model and that of a model with multi-target cell compartments may not differ substantially unless a large fraction of the total target cells in the modified model remain uninfected around peak viral load. Another modelling limitation is that possible immunomodulation induced by treatment was not modelled. That is, if anti-SARS-CoV-2 drugs induce immunomodulation as bystander effects, late initiation of treatments might still have the potential to reduce viral load, which is not reflected in our model [24]. We further compared the results of the model we used in this study with two other extended models, which have been used to describe virus dynamics of SARS-CoV-2 and other viruses, to check whether our model is appropriate: one included the effect of interferons produced by infected cells [46] and the other included the eclipse phase of infection [46, 47]. We fit these models to the data and used model selection theory to compare the models based on the Bayesian information criteria (BIC) and corrected Bayesian information criteria (BICc). BIC and BICc among the three models were comparable. In addition, given limited data (i.e., only viral load data were available), we believe using a minimal model is appropriate at this stage of knowledge. At such time that further data and appropriate scientific information about infection dynamics becomes available, more complex models may be able to capture additional details of within-host viral dynamics. Second, we did not use viral load data under treatment to evaluate our model because such data were not sufficiently available. Estimating antiviral effects from such data and using that in the

509 sample size calculation would strengthen our approach, but we need to wait until such
510 data are accumulated.

511 Future study should include development of a similar sample size calculation
512 framework for different types of antiviral treatment. Although we focused on drugs
513 inhibiting virus replication, there are different classes of drugs such as viral entry
514 inhibitors (e.g., hydroxychloroquine and camostat) and immunomodulators (e.g.,
515 interferon and the related agents) [48].

516 Along with vaccines, developing effective antiviral drugs is urgently needed. At
517 present, most of the randomized controlled trials have failed to identify effective antiviral
518 agents against SARS-CoV-2. However, this might not be because the antiviral drugs
519 are not effective, but because of imperfect design of the clinical studies. The timing of
520 treatment initiation and virus dynamics should be accounted for in the study design (i.e.,
521 sample size and inclusion-exclusion criteria). We further believe our approach is
522 informative for determining treatment strategy in clinical settings.

523

524 **Acknowledgments:**

525 **Funding:** a Grant-in-Aid for JSPS Research Fellows 19J12319 (to S.I.), Scientific
526 Research (KAKENHI) B 18KT0018 (to S.I.), 18H01139 (to S.I.), 16H04845 (to S.I.),
527 17H04085 (to K.W.), Scientific Research in Innovative Areas 20H05042 (to S.I.),
528 19H04839 (to S.I.), 18H05103 (to S.I.); AMED CREST 19gm1310002 (to S.I.); AMED J-
529 PRIDE 19fm0208006s0103 (to S.I.), 19fm0208014h0003 (to S.I.), 19fm0208019h0103
530 (to S.I.), 19fm0208019j0003 (to K.W.); AMED Research Program on HIV/AIDS
531 19fk0410023s0101 (to S.I.); Research Program on Emerging and Re-emerging

532 Infectious Diseases 19fk0108050h0003 (to S.I.), 19fk0108156h0001 (to S.I.),
533 20fk0108140s0801 (to S.I.) and 20fk0108413s0301 (to S.I.); Program for Basic and
534 Clinical Research on Hepatitis 19fk0210036h0502 (to S.I.), 19fk0210036j0002 (to
535 K.W.); Program on the Innovative Development and the Application of New Drugs for
536 Hepatitis B 19fk0310114h0103 (to S.I.), 19fk0310114j0003 (to K.W.),
537 19fk0310101j1003 (to K.W.) , 19fk0310103j0203 (to K.W.); JST MIRAI (to S.I. and
538 K.W.); JST CREST (to S.I. and K.W.); Moonshot R&D Grant Number JPMJMS2021 (to
539 K.A. and S.I.) and JPMJMS2025 (to S.I.); Mitsui Life Social Welfare Foundation (to S.I.
540 and K.W.); Shin-Nihon of Advanced Medical Research (to S.I.); Suzuken Memorial
541 Foundation (to S.I.); Life Science Foundation of Japan (to S.I.); SECOM Science and
542 Technology Foundation (to S.I.); The Japan Prize Foundation (to S.I.); Toyota Physical
543 and Chemical Research Institute (to S.I.); The Yasuda Medical Foundation (to K.W.);
544 Smoking Research Foundation (to K.W.); and The Takeda Science Foundation (to
545 K.W.); the U.S. National Science Foundation PHY-2031756 (to A.S.P.); National
546 Institutes of Health R01-OD011095 and R01-AI028433 (to A.S.P.); and Los Alamos
547 National Laboratory LDRD Program grant 20200695ER (to A.S.P.); **Author
548 contributions:** Conceptualization, K.E. and S.I.; investigation, S. Iwanami, K.E., K.S.K.,
549 K.N., Y.F., S.I.; supervision, K.E., A.S.P, and S.I.; writing, original draft, S. Iwanami,
550 K.E., K.F., A.S.P, and S.I.; writing–review and editing, all authors; funding acquisition:
551 K.W., K.A., A.S.P., and S.I.; **Competing interests:** Authors declare no competing
552 interests.; **Data and materials availability:** All data is available in the main text or the
553 supplementary materials.
554

References

1. Pushpakom S, Iorio F, Eyers PA, Escott KJ, Hopper S, Wells A, et al. Drug repurposing: progress, challenges and recommendations. Nat Rev Drug Discov. 2019;18(1):41-58. Epub 2018/10/13. doi: 10.1038/nrd.2018.168. PubMed PMID: 30310233.
2. Ohashi H, Watashi K, Saso W, Shionoya K, Iwanami S, Hirokawa T, et al. Multidrug treatment with nelfinavir and cepharanthine against COVID-19. bioRxiv. 2020:2020.04.14.039925. doi: 10.1101/2020.04.14.039925.
3. Williamson BN, Feldmann F, Schwarz B, Meade-White K, Porter DP, Schulz J, et al. Clinical benefit of remdesivir in rhesus macaques infected with SARS-CoV-2. Nature. 2020;585(7824):273-6. doi: 10.1038/s41586-020-2423-5.
4. Cao B, Wang Y, Wen D, Liu W, Wang J, Fan G, et al. A Trial of Lopinavir-Ritonavir in Adults Hospitalized with Severe Covid-19. N Engl J Med. 2020. Epub 2020/03/19. doi: 10.1056/NEJMoa2001282. PubMed PMID: 32187464; PubMed Central PMCID: PMCPMC7121492.
5. Wang Y, Zhang D, Du G, Du R, Zhao J, Jin Y, et al. Remdesivir in adults with severe COVID-19: a randomised, double-blind, placebo-controlled, multicentre trial. The Lancet. 2020.
6. Borba MGS, Val FFA, Sampaio VS, Alexandre MAA, Melo GC, Brito M, et al. Effect of High vs Low Doses of Chloroquine Diphosphate as Adjunctive Therapy for Patients Hospitalized With Severe Acute Respiratory Syndrome Coronavirus 2 (SARS-CoV-2) Infection: A Randomized Clinical Trial. JAMA Netw Open. 2020;3(4):e208857. Epub 2020/04/28. doi: 10.1001/jamanetworkopen.2020.8857. PubMed PMID: 32339248.
7. Cai Q, Yang M, Liu D, Chen J, Shu D, Xia J, et al. Experimental Treatment with Favipiravir for COVID-19: An Open-Label Control Study. Engineering (Beijing). 2020. Epub 2020/04/30. doi: 10.1016/j.eng.2020.03.007. PubMed PMID: 32346491; PubMed Central PMCID: PMCPMC7185795.
8. Sanders JM, Monogue ML, Jodlowski TZ, Cutrell JB. Pharmacologic Treatments for Coronavirus Disease 2019 (COVID-19). JAMA. 2020. doi: 10.1001/jama.2020.6019.
9. Beigel JH, Tomashek KM, Dodd LE, Mehta AK, Zingman BS, Kalil AC, et al. Remdesivir for the Treatment of Covid-19 — Preliminary Report. New Engl J Med. 2020. doi: 10.1056/NEJMoa2007764.
10. Lu H. Drug treatment options for the 2019-new coronavirus (2019-nCoV). Biosci Trends. 2020. Epub 2020/01/31. doi: 10.5582/bst.2020.01020. PubMed PMID: 31996494.
11. Yao TT, Qian JD, Zhu WY, Wang Y, Wang GQ. A Systematic Review of Lopinavir Therapy for SARS Coronavirus and MERS Coronavirus-A Possible Reference for Coronavirus Disease-19 Treatment Option. J Med Virol. 2020. Epub 2020/02/28. doi: 10.1002/jmv.25729. PubMed PMID: 32104907.
12. Bauchner H, Fontanarosa PB. Randomized Clinical Trials and COVID-19: Managing Expectations. JAMA. 2020;323(22):2262. doi: 10.1001/jama.2020.8115.
13. Ejima K, Li P, Smith DL, Jr., Nagy TR, Kadish I, van Groen T, et al. Observational research rigour alone does not justify causal inference. European journal of clinical investigation. 2016;46(12):985-93. Epub 2016/10/30. doi: 10.1111/eci.12681. PubMed PMID: 27711975; PubMed Central PMCID: PMCPMC5118066.
14. Gautret P, Lagier JC, Parola P, Hoang VT, Meddeb L, Mailhe M, et al. Hydroxychloroquine and azithromycin as a treatment of COVID-19: results of an open-label non-randomized clinical trial. Int J Antimicrob Agents. 2020:105949. Epub 2020/03/25. doi:

10.1016/j.ijantimicag.2020.105949. PubMed PMID: 32205204; PubMed Central PMCID: PMCPMC7102549.

15. Geleris J, Sun Y, Platt J, Zucker J, Baldwin M, Hripcsak G, et al. Observational Study of Hydroxychloroquine in Hospitalized Patients with Covid-19. N Engl J Med. 2020. Epub 2020/05/08. doi: 10.1056/NEJMoa2012410. PubMed PMID: 32379955.

16. Ikeda H, Nakaoka S, de Boer RJ, Morita S, Misawa N, Koyanagi Y, et al. Quantifying the effect of Vpu on the promotion of HIV-1 replication in the humanized mouse model. Retrovirology. 2016;13:23. Epub 2016/04/19. doi: 10.1186/s12977-016-0252-2. PubMed PMID: 27086687; PubMed Central PMCID: PMCPMC4834825.

17. Martyushev A, Nakaoka S, Sato K, Noda T, Iwami S. Modelling Ebola virus dynamics: Implications for therapy. Antiviral Res. 2016;135:62-73. Epub 2016/10/28. doi: 10.1016/j.antiviral.2016.10.004. PubMed PMID: 27743917.

18. Best K, Guedj J, Madelain V, de Lamballerie X, Lim SY, Osuna CE, et al. Zika plasma viral dynamics in nonhuman primates provides insights into early infection and antiviral strategies. Proc Natl Acad Sci U S A. 2017;114(33):8847-52. Epub 2017/08/03. doi: 10.1073/pnas.1704011114. PubMed PMID: 28765371; PubMed Central PMCID: PMCPMC5565429.

19. Young BE, Ong SWX, Kalimuddin S, Low JG, Tan SY, Loh J, et al. Epidemiologic Features and Clinical Course of Patients Infected With SARS-CoV-2 in Singapore. JAMA. 2020;323(15):1488. doi: 10.1001/jama.2020.3204.

20. Zou L, Ruan F, Huang M, Liang L, Huang H, Hong Z, et al. SARS-CoV-2 Viral Load in Upper Respiratory Specimens of Infected Patients. N Engl J Med. 2020. Epub 2020/02/20. doi: 10.1056/NEJMc2001737. PubMed PMID: 32074444.

21. Kim ES, Chin BS, Kang CK, Kim NJ, Kang YM, Choi J-P, et al. Clinical Course and Outcomes of Patients with Severe Acute Respiratory Syndrome Coronavirus 2 Infection: a Preliminary Report of the First 28 Patients from the Korean Cohort Study on COVID-19. Journal of Korean Medical Science. 2020;35(13). doi: 10.3346/jkms.2020.35.e142.

22. Wolfel R, Corman VM, Guggemos W, Seilmaier M, Zange S, Muller MA, et al. Virological assessment of hospitalized patients with COVID-2019. Nature. 2020. Epub 2020/04/03. doi: 10.1038/s41586-020-2196-x. PubMed PMID: 32235945.

23. Ikeda H, Nakaoka S, de Boer RJ, Morita S, Misawa N, Koyanagi Y, et al. Quantifying the effect of Vpu on the promotion of HIV-1 replication in the humanized mouse model. Retrovirology. 2016;13(1):23. doi: 10.1186/s12977-016-0252-2.

24. Kim KS, Ejima K, Ito Y, Iwanami S, Ohashi H, Koizumi Y, et al. Modelling SARS-CoV-2 Dynamics: Implications for Therapy. medRxiv. 2020:2020.03.23.20040493. doi: 10.1101/2020.03.23.20040493.

25. Perelson AS. Modelling viral and immune system dynamics. Nature Rev Immunol. 2002;2(1):28-36. doi: 10.1038/nri700.

26. Gonçalves A, Bertrand J, Ke R, Comets E, de Lamballerie X, Malvy D, et al. Timing of antiviral treatment initiation is critical to reduce SARS-CoV-2 viral load. CPT Pharmacometrics Syst Pharmacol. 2020;**9**, 509-514. doi: 10.1002/psp4.12543.

27. Traynard P, Ayral G, Twarogowska M, Chauvin J. Efficient Pharmacokinetic Modeling Workflow With the MonolixSuite: A Case Study of Remifentanil. CPT: Pharmacometrics & Syst Pharmacol. 2020;9(4):198-210.

28. Adeline Samson, Marc Lavielle, France Mentré. Extension of the SAEM algorithm to left-censored data in nonlinear mixed-effects model: Application to HIV dynamics model. Computational Statistics & Data Analysis. 2006;51(3):1562-74. doi: 10.1016/j.csda.2006.05.007.
29. Ward Jr JH. Hierarchical grouping to optimize an objective function. Journal of the American statistical association. 1963;58(301):236-44.
30. Virtanen P, Gommers R, Oliphant TE, Haberland M, Reddy T, Cournapeau D, et al. SciPy 1.0: fundamental algorithms for scientific computing in Python. Nature Methods. 2020;17(3):261-72. doi: 10.1038/s41592-019-0686-2.
31. Bi Q, Wu Y, Mei S, Ye C, Zou X, Zhang Z, et al. Epidemiology and transmission of COVID-19 in 391 cases and 1286 of their close contacts in Shenzhen, China: a retrospective cohort study. Lancet Infect Dis. 2020. Epub 2020/05/01. doi: 10.1016/s1473-3099(20)30287-5. PubMed PMID: 32353347; PubMed Central PMCID: PMCPMC7185944.
32. Monto AS, Fleming DM, Henry D, de Groot R, Makela M, Klein T, et al. Efficacy and safety of the neuraminidase inhibitor zanamivirin the treatment of influenza A and B virus infections. J Infect Dis. 1999;180(2):254-61. Epub 1999/07/09. doi: 10.1086/314904. PubMed PMID: 10395837.
33. Wood MJ, Shukla S, Fiddian AP, Crooks RJ. Treatment of acute herpes zoster: effect of early (< 48 h) versus late (48-72 h) therapy with acyclovir and valaciclovir on prolonged pain. J Infect Dis. 1998;178 Suppl 1:S81-4. Epub 1998/12/16. doi: 10.1086/514271. PubMed PMID: 9852981.
34. Nicholson KG, Aoki FY, Osterhaus AD, Trottier S, Carewicz O, Mercier CH, et al. Efficacy and safety of oseltamivir in treatment of acute influenza: a randomised controlled trial. Neuraminidase Inhibitor Flu Treatment Investigator Group. Lancet. 2000;355(9218):1845-50. Epub 2000/06/24. doi: 10.1016/s0140-6736(00)02288-1. PubMed PMID: 10866439.
35. Goyal A, Cardozo-Ojeda EF, Schiffer JT. Potency and timing of antiviral therapy as determinants of duration of SARS-CoV-2 shedding and intensity of inflammatory response. Sci Adv. 2020;6(47):eabc7112. doi: 10.1126/sciadv.abc7112.
36. Wang F, Nie J, Wang H, Zhao Q, Xiong Y, Deng L, et al. Characteristics of peripheral lymphocyte subset alteration in COVID-19 pneumonia. J Infect Dis. 2020. Epub 2020/04/01. doi: 10.1093/infdis/jiaa150. PubMed PMID: 32227123; PubMed Central PMCID: PMCPMC7184346.
37. Bost P, Giladi A, Liu Y, Bendjelal Y, Xu G, David E, et al. Host-Viral Infection Maps Reveal Signatures of Severe COVID-19 Patients. Cell. 2020;181(7):1475-88.e12. Epub 2020/06/02. doi: 10.1016/j.cell.2020.05.006. PubMed PMID: 32479746; PubMed Central PMCID: PMCPMC7205692.
38. Fry AM, Goswami D, Nahar K, Sharmin AT, Rahman M, Gubareva L, et al. Efficacy of oseltamivir treatment started within 5 days of symptom onset to reduce influenza illness duration and virus shedding in an urban setting in Bangladesh: a randomised placebo-controlled trial. Lancet Infect Dis. 2014;14(2):109-18. Epub 2013/11/26. doi: 10.1016/s1473-3099(13)70267-6. PubMed PMID: 24268590.
39. Shufa Zheng, Jian Fan, Fei Yu, Baihuan Feng, Bin Lou, Qianda Zou, et al. Viral load dynamics and disease severity in patients infected with SARS-CoV-2 in Zhejiang province, China, January-March 2020: retrospective cohort study. BMJ. 2020:m1443. doi: 10.1136/bmj.m1443.

40. Long Q-X, Tang X-J, Shi Q-L, Li Q, Deng H-J, Yuan J, et al. Clinical and immunological assessment of asymptomatic SARS-CoV-2 infections. Nature Medicine. 2020;26(8):1200-4. doi: 10.1038/s41591-020-0965-6.
41. Ryan TP. Sample size determination and power: John Wiley & Sons; 2013.
42. Liu Y, Yan L-M, Wan L, Xiang T-X, Le A, Liu J-M, et al. Viral dynamics in mild and severe cases of COVID-19. The Lancet Infectious Diseases. 2020;20(6):656-7. doi: 10.1016/s1473-3099(20)30232-2.
43. Pujadas E, Chaudhry F, Mcbride R, Richter F, Zhao S, Wajnberg A, et al. SARS-CoV-2 viral load predicts COVID-19 mortality. The Lancet Respiratory Medicine. 2020;8(9):e70. doi: 10.1016/s2213-2600(20)30354-4.
44. Néant N, Lingas G, Le Hingrat Q, Ghosn J, Engelmann I, Lepiller Q, et al. Modeling SARS-CoV-2 viral kinetics and association with mortality in hospitalized patients from the French COVID cohort. Proc Natl Acad Sci USA. 2021;118(8):e2017962118. doi: 10.1073/pnas.2017962118.
45. Ziegler CGK, Allon SJ, Nyquist SK, Mbano IM, Miao VN, Tzouanas CN, et al. SARS-CoV-2 Receptor ACE2 Is an Interferon-Stimulated Gene in Human Airway Epithelial Cells and Is Detected in Specific Cell Subsets across Tissues. Cell. 2020. Epub 2020/05/16. doi: 10.1016/j.cell.2020.04.035. PubMed PMID: 32413319.
46. Prasith Baccam, Catherine Beauchemin, A. Macken C, G. Hayden F, S. Perelson A. Kinetics of Influenza A Virus Infection in Humans. J Virol. 2006;80(15):7590-9. doi: 10.1128/jvi.01623-05.
47. Antonio Gonçalves, Julie Bertrand, Ruian Ke, Emmanuelle Comets, Xavier Lamballerie, Denis Malvy, et al. Timing of Antiviral Treatment Initiation is Critical to Reduce SARS‐CoV‐2 Viral Load. CPT: Pharmacometrics & Systems Pharmacology. 2020. doi: 10.1002/psp4.12543.
48. Santos J, Brierley S, Gandhi MJ, Cohen MA, Moschella PC, Declan ABL. Repurposing Therapeutics for Potential Treatment of SARS-CoV-2: A Review. Viruses. 2020;12(7). Epub 2020/07/08. doi: 10.3390/v12070705. PubMed PMID: 32629804.

717 # Supporting information

718 Supplementary Text

719 Figures S1-S4

720 Tables S1-S4

721

Figures

Fig. 1. Observed and fitted viral load data for individual patients. Viral loads were measured using nasal swabs (China), pharyngeal swabs (Germany), and nasopharyngeal swabs (Singapore and France) for hospitalized SARS-CoV-2-infected patients. Note that the detection limits of the PCR assay for SARS-CoV-2 were 68.0 copies/ml (Singapore and Korea) 15.3 copies/ml (China) and 33.3 copies/ml (Germany), respectively, and are shown as dotted horizontal lines. The closed dots and curves correspond to the observed and the estimated viral load for each patient using their individual parameters given in **Table S2**, respectively. Shaded regions correspond to 95% predictive intervals. Different colors of the dots and the lines (light blue, black, and pink) correspond to the three different types of patients characterized by rapid, medium, and slow viral load decay, respectively. The red dots represent the data at or under the detection limit regardless of the group. Patient IDs are the same as in the original papers if available.

Fig. 2. Characterizing and clustering COVID-19 patients using viral load data. (A) Schematic illustration for data fitting with a virus dynamics model. Longitudinal SARS-CoV-2 RNA load data (i.e., clinical data) were extracted from published papers. The data were analyzed by the mathematical model, and then virus dynamics parameters were estimated for each patient (i.e., characterizing). Daily viral load since symptom onset for each patient was simulated by running the model with the estimated parameters. (B) Clustering patients using daily viral load. Daily viral load obtained through simulation was used for clustering of the 30 patients. In the dendrogram, the height from the bottom to the point where two or more patients are joined indicates the

745 distance (i.e., dissimilarity) between patients. For example, “Singapore 11” and
746 “Germany 2” are very close and those are far from “Singapore 6.” As a result, three
747 different patient groups were identified and “China O” was detected as an outlier. The
748 heatmap next to the dendrogram (“Virus dynamics parameters”) shows the estimated
749 parameters and initial condition $(\gamma, \beta, V(0), \delta)$ for each patient. Light blue and pink
750 correspond to high and low values, respectively. Statistically significant between-group
751 differences were found in the maximum rate constant for viral replication, γ (ANOVA p-
752 value: 3.61×10^{-3}), and the death rate of virus-producing cells, δ (ANOVA p-value:
753 3.23×10^{-13}), moreover there were statistical differences between all pair groups for δ.
754 The death rate is highlighted by the dotted square. The right heatmap shows the daily
755 viral load for each patient. Green and purple correspond to high and low values,
756 respectively. “Group 1” maintained a high viral load for a longer period compared with
757 the other groups.

758 **Fig. 3. Patient variability and difference in therapeutic response.** (A) Viral load
759 trajectories since symptom onset for the three groups (black: medium decay group, light
760 blue: rapid decay group, pink: slow decay group) obtained through simulation (without
761 antiviral treatment). (B) Viral load trajectories since symptom onset for the three groups
762 under antiviral treatment with different inhibition rates and different timing of treatment
763 initiation. The left three panels are viral load trajectories when the treatment is initiated
764 at 0.5 days (“Early initiation”) since symptom onset. The right three panels are vial load
765 trajectories when treatment is initiated at 5 days (“Late initiation”) since symptom onset.
766 Blue and red dotted lines correspond to the trajectories with 50% and 99% inhibition

767 rate, respectively. The bolded lines are the trajectory without treatment shown for
768 comparison. The dotted horizontal lines are the detection limit (D.L.).

769 **Fig. 4. Duration of virus shedding in the three different groups.** (A) The relative
770 density distributions of duration of virus shedding since symptom onset for the three
771 groups (light pink: medium decay group, light blue: rapid decay group, pink: slow decay
772 group) without treatment obtained through simulation. (B) The relative density
773 distributions of duration of virus shedding since symptom onset for the three groups
774 under antiviral treatment with different inhibition rates and different timing of treatment
775 initiation. The left three panels are when antiviral treatment is initiated at 0.5 days
776 ("Early initiation") since symptom onset. The red dotted line corresponds to the
777 distribution with a 99% inhibition rate. The distribution without treatment is shown in the
778 back for comparison. The right three panels are when antiviral treatment is initiated at 5
779 days ("Late initiation") since symptom onset. The distributions are represented as
780 'relative density' to reflect different proportions of the three groups.

781 **Fig. 5. Simulation mimicking randomized controlled trial for anti-SARS-CoV-2.** (A)
782 Schematic illustration for the simulation mimicking randomized controlled trials for
783 antiviral drugs. 20,000 parameter sets were sampled from the estimated parameter
784 distributions. The parameter sets were randomized into control ("No treatment", 10,000
785 individuals in total) or treatment ("Anti-SARS-CoV-2 treatment", 10,000 individuals in
786 total) groups. For the treatment group, the treatment is initiated randomly to reflect the
787 delay of treatment initiation since symptom onset. We have also used a truncated
788 distribution (red area) to mimic the randomized controlled trials including only patients
789 recruited and treated early ("Early initiation"). Then the outcomes (duration of virus

790 shedding and the cumulative viral load in log scale) were calculated for each patient. (B)
791 The distributions of duration of virus shedding for patients without and with treatment
792 are shown in black and red curves, respectively. For antiviral treatment, a 99% inhibition
793 rate of virus replication was assumed. The red dotted curve is when all patients are
794 included regardless of the timing of recruitment and treatment initiation. The red dashed
795 curve is the case when only patients recruited and treated within 0.5 days since
796 symptom onset are included. (C) Means and standard deviation of the duration of virus
797 shedding under different inclusion criteria (not treated, included regardless of the timing
798 of recruitment and treatment initiation, early treatment initiation [within 0.5, 1, 2, 3, 4,
799 days since symptom onset]) are shown.

Supporting information for

Detection of significant antiviral drug effects on COVID-19 with reasonable sample sizes in randomized controlled trials: a modeling study combined with clinical data

Shoya Iwanami, Keisuke Ejima, Kwang Su Kim, Koji Noshita, Yasuhisa Fujita, Taiga Miyazaki, Shigeru Kohno, Yoshitsugu Miyazaki, Shimpei Morimoto, Shinji Nakaoka, Yoshiki Koizumi, Yusuke Asai, Kazuyuki Aihara, Koichi Watashi, Robin N. Thompson, Kenji Shibuya, Katsuhito Fujiu, Alan S. Perelson, Shingo Iwami*, Takaji Wakita

*Correspondence to: iwamishingo@gmail.com

This PDF file includes:

Figs. S1 to S4
Tables S1 to S4

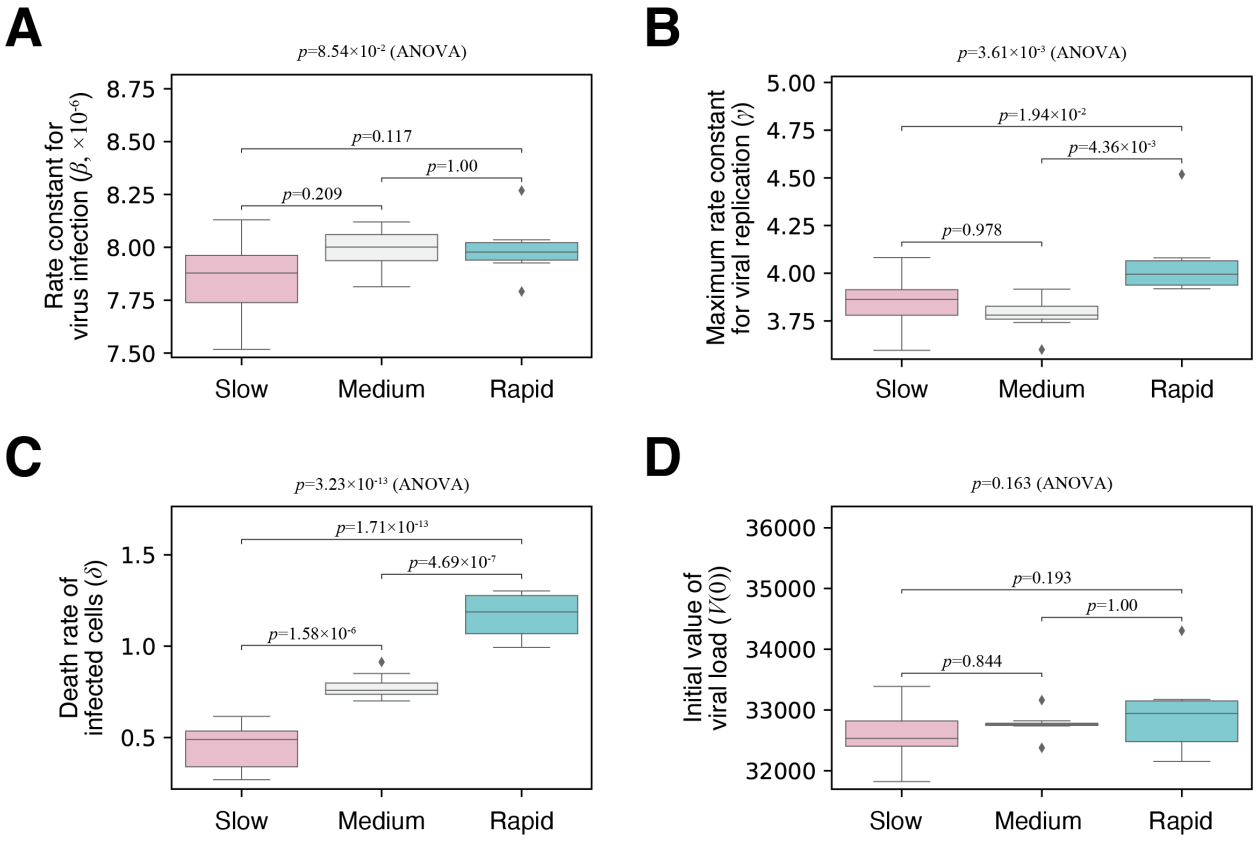

Fig. S1. Estimated parameters of the mathematical model in the three different viral load decay groups. Boxplots of estimates of (A) the rate constant for virus infection, β; (B) the maximum rate constant for viral replication, γ; (C) the death rate of virus-producing cells, δ; and (D) viral load at symptom onset, $V(0)$, respectively. Estimated parameter distributions between the three groups with different viral load dynamics (slow, medium, and rapid viral load decay groups) were compared by ANOVA. Pairwise comparison was subsequently performed using Student's *t* test. The p-values of the pairwise Student's *t* test were adjusted by the Bonferroni correction.

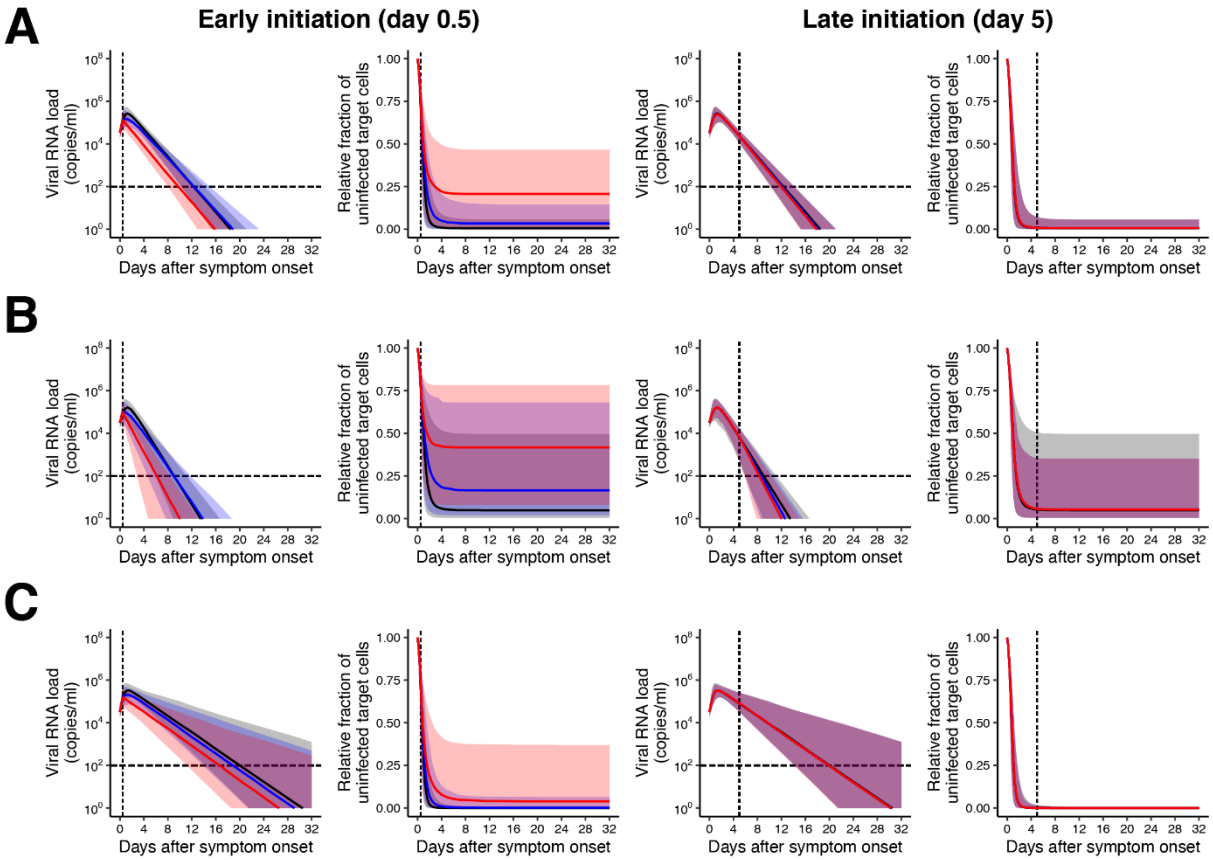

Fig. S2. Expected virus dynamics under an antiviral treatment blocking viral replication. The antiviral treatment was assumed to be initiated after 0.5 or 5 days (named early and late initiations, respectively) from symptom onset with 99% and 50% inhibition rates (named high and low antiviral effects, respectively) for patients with (A) medium, (B) rapid, and (C) slow viral load decay. Left and right panels in each group show the viral loads, $V(t)$, and the relative fraction of uninfected target cells, $f(t)$. The black and colored solid lines correspond to the mean of the values without and with the therapies (red: high, blue: low antiviral effects), respectively. The shadowed regions correspond to the 95% predictive intervals.

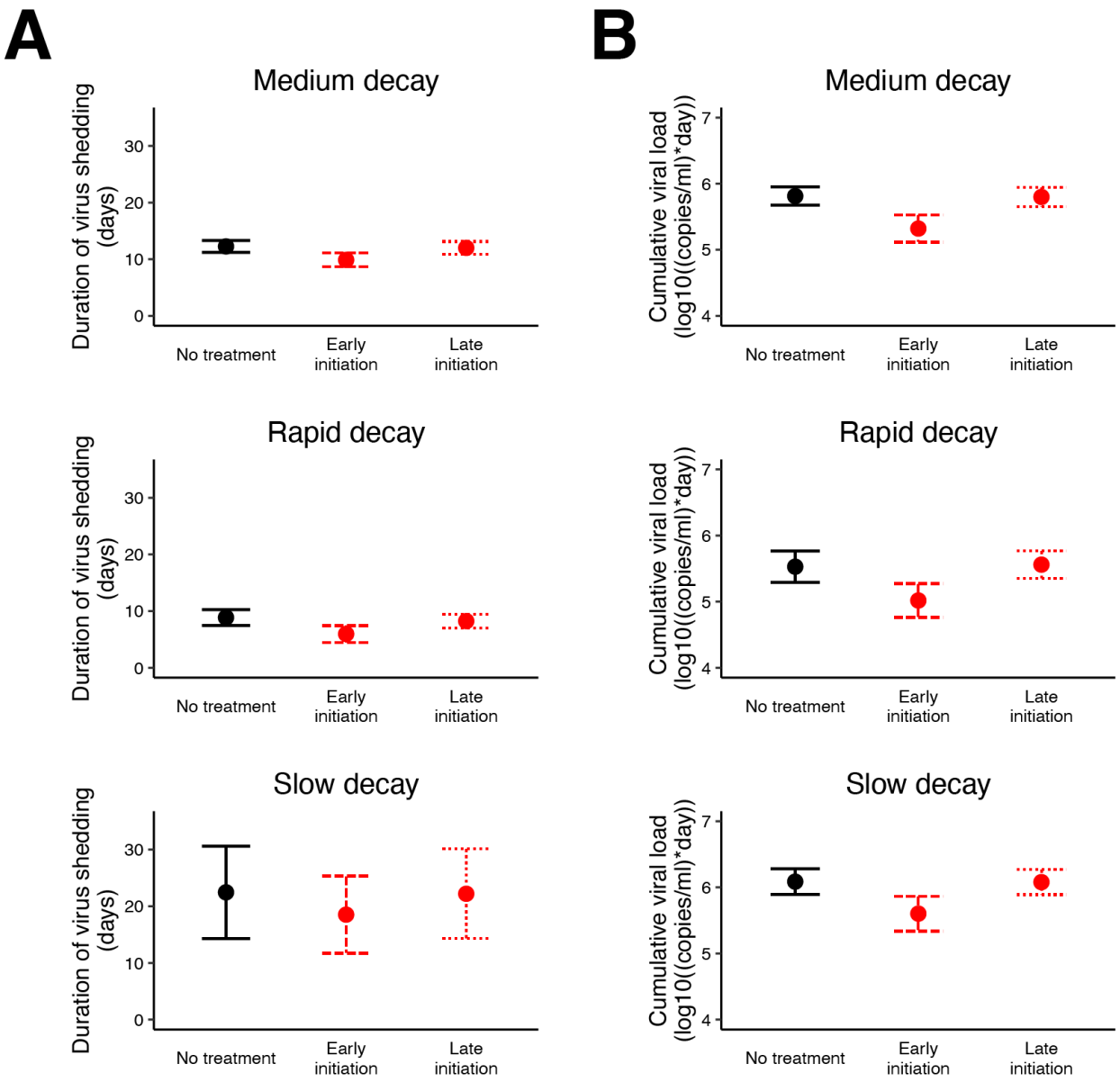

Fig. S3. Distribution of duration of virus shedding and cumulative viral load. (A) Duration of virus shedding and (B) cumulative viral load of SARS-CoV-2 for different types of patients (medium, rapid, and slow decay) with and without treatment. 'Early initiation' and 'Late initiation' means the early and the late treatment initiation (0.5 or 5 days after symptom onset). The dots and error bars represent the mean and the standard deviation.

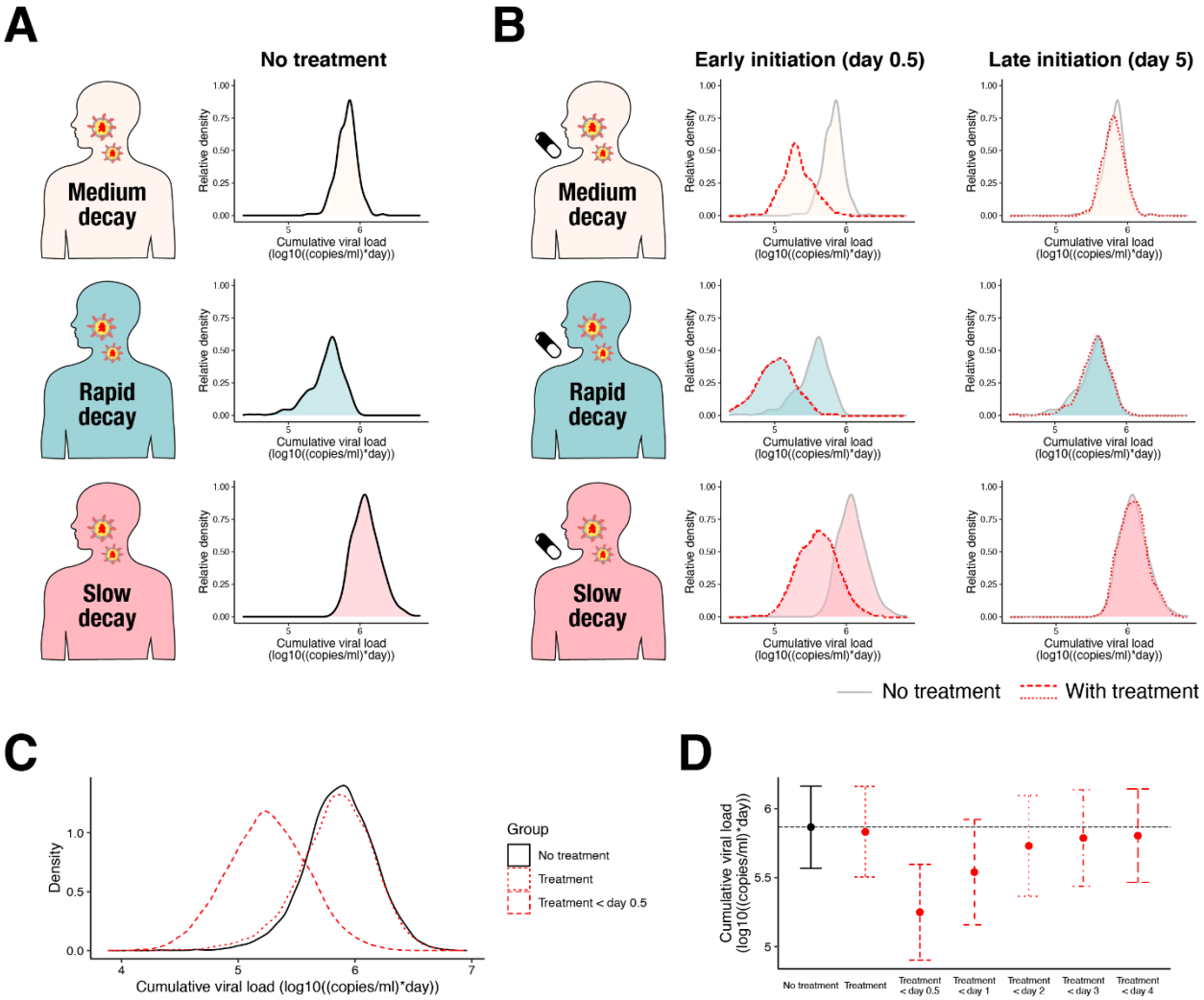

Fig. S4. Cumulative viral load in the three different groups. (A) The relative density distributions of cumulative viral load for the three groups (light pink: medium decay group, light blue: rapid decay group, pink: slow decay group) without treatment obtained through simulation. (B) The relative density distributions of cumulative viral load (in log scale) for the three groups under antiviral treatment with different inhibition rate and different timing of treatment initiation. The left three panels are when antiviral treatment is initiated at 0.5 days ("Early initiation") since symptom onset. The red dotted line corresponds to the distribution with 99% inhibition rate. The distribution without treatment is shown in the back for comparison. The right three panels are when antiviral treatment is initiated at 5 days ("Late initiation") since symptom onset. The distributions are represented as 'relative density' to reflect different proportions of the three groups. (C) The distributions of cumulative viral load for patients without and with treatment are shown in black and red curves, respectively. The red dotted curve is when all patients are included regardless of the timing of recruiting and treatment initiation. The red dashed curve is the case for patients who were recruited and who received treatment

within 0.5 days since symptom onset only. (D) Means and standard deviation of the cumulative viral load under different inclusion criteria (not treated, included regardless of the timing of recruiting and treatment initiation, early treatment initiation [within 0.5, 1, 2, 3, 4 days since symptom onset]) are shown.

Table S1. Summary of clinical trials for antiviral drugs for SARS-CoV-2: The current major clinical studies for antiviral treatment of SARS-CoV-2 were investigated and their information were summarized on 22 May 2020.

Treatment	Study design[$]	Timing of initiation since onset (days)	Sample size (control/treatment)	Primary outcome[*]	Effective[#]	Reference	Peer-reviewed
Lopinavir/ritonavir	RCT	13 (IQR: 11-16)	99/100	1	No	(*1*)	Yes
Remdesivir	RCT	10 (IQR: 9-12)	79/158	1	No	(*2*)	Yes
Remdesivir	RCT	9 (IQR: 6-12)	521/538	1	Yes	(*3*)	Yes
Hydroxychloroquine	RCT	Not reported	31/31	1	Yes	(*4*)	No
Hydroxychloroquine	RCT	16.6 (SD: 10.5)	75/75	2	No	(*5*)	Yes
Lopinavir/ritonavir	RCT	3.5 (IQR: 2-6)	17/34	2	No	(*6*)	No
Arbidol	RCT	6 (IQR: 2-8)	17/35	2	No	(*6*)	No
Remdesivir	OS	12 (IQR: 9-15)	53	1,3	-	(*7*)	Yes
Hydroxychloroquine	OS	4.1 (SD: 2.6)	16/20	2	Yes	(*8*)	Yes
Hydroxychloroquine	OS	Not reported	565/811	1,3	No	(*9*)	Yes
Hydroxychloroquine and azithromycin	OS	4.9 (SD: 3.6)	80	1,2	-	(*10*)	Yes
Meplazumab	OS	Not reported	11/17	2	Yes	(*11*)	No

$ RCT: randomized control trial, OS: observational study

* 1. Clinical improvement/recovery, 2. Duration of virus shedding, 3. Mortality.

Whether the primary outcome is statistically significantly different between control and treatment group. '-' denotes no statistical test was performed because it is a single-arm study (i.e., no control group).

Table S2. Estimated parameters for each patient (mode and 95% credible intervals): The conditional modes of the individual parameters for each patient were estimated as Empirical Bayes Estimates and summarized. The patient type was based on the three groups identified by hierarchical clustering of the reconstructed daily viral load data.

Patient ID	γ (day^{-1})	β ((RNA copies/ml)$^{-1}$day^{-1})	δ (day^{-1})	$V(0)$ (RNA copies/ml)	Patient type
Germany					
1	$3.74\ (2.25-5.99)$	$8.12\ (5.48-11.2)\times 10^{-6}$	$0.75\ (0.68-0.93)$	$3.32\ (1.84-5.70)\times 10^{4}$	Medium
2	$4.05\ (2.81-5.97)$	$7.79\ (5.95-10.2)\times 10^{-6}$	$1.08\ (0.88-1.34)$	$3.23\ (1.71-4.66)\times 10^{4}$	Rapid
3	$3.92\ (1.89-6.35)$	$8.27\ (6.08-10.9)\times 10^{-6}$	$1.30\ (1.07-2.06)$	$3.43\ (1.89-5.44)\times 10^{4}$	Rapid
4	$4.08\ (2.80-6.05)$	$7.93\ (6.07-10.3)\times 10^{-6}$	$1.27\ (0.99-1.92)$	$3.31\ (2.07-6.37)\times 10^{4}$	Rapid
7	$3.92\ (2.45-5.36)$	$7.81\ (5.82-11.2)\times 10^{-7}$	$0.91\ (0.80-1.29)$	$3.28\ (1.65-5.27)\times 10^{4}$	Medium
8	$3.77\ (2.34-5.64)$	$8.04\ (5.57-10.9)\times 10^{-6}$	$0.75\ (0.67-0.84)$	$3.28\ (1.95-5.82)\times 10^{4}$	Medium
10	$3.90\ (2.59-5.85)$	$7.74\ (5.60-11.4)\times 10^{-7}$	$0.49\ (0.46-0.55)$	$3.18\ (1.75-6.22)\times 10^{4}$	Slow
14	$4.06\ (2.97-6.17)$	$7.95\ (5.89-11.1)\times 10^{-6}$	$1.28\ (1.02-1.75)$	$3.28\ (1.95-5.82)\times 10^{4}$	Rapid
Korea					
13	$3.93\ (2.39-6.18)$	$8.02\ (5.89-10.4)\times 10^{-6}$	$0.99\ (0.79-1.36)$	$3.31\ (1.58-5.97)\times 10^{4}$	Rapid
15	$3.91\ (2.13-6.10)$	$7.83\ (5.80-11.1)\times 10^{-7}$	$0.78\ (0.55-0.93)$	$3.24\ (1.94-6.09)\times 10^{4}$	Medium
Singapore					
2	$3.78\ (2.47-6.02)$	$7.96\ (6.15-10.6)\times 10^{-6}$	$0.61\ (0.51-0.68)$	$3.26\ (1.83-5.90)\times 10^{4}$	Slow
3	$4.00\ (2.75-6.36)$	$7.74\ (5.77-10.4)\times 10^{-6}$	$0.33\ (0.24-0.38)$	$3.26\ (1.93-5.62)\times 10^{4}$	Slow
4	$3.83\ (2.24-6.46)$	$7.88\ (6.00-10.5)\times 10^{-6}$	$0.62\ (0.47-0.69)$	$3.25\ (1.82-5.46)\times 10^{4}$	Slow
6	$3.86\ (2.42-6.43)$	$7.93\ (5.47-11.0)\times 10^{-6}$	$0.37\ (0.26-0.43)$	$3.28\ (2.01-6.64)\times 10^{4}$	Slow
8	$3.76\ (2.45-5.87)$	$8.04\ (6.01-10.3)\times 10^{-6}$	$0.41\ (0.35-0.45)$	$3.34\ (1.63-6.28)\times 10^{4}$	Slow
9	$3.60\ (2.39-4.94)$	$8.13\ (6.00-10.5)\times 10^{-6}$	$0.27\ (0.22-0.31)$	$3.28\ (1.61-5.53)\times 10^{4}$	Slow
11	$3.94\ (2.35-6.19)$	$8.04\ (6.58-11.2)\times 10^{-6}$	$1.14\ (0.90-1.76)$	$3.32\ (1.74-6.53)\times 10^{4}$	Rapid
12	$3.77\ (2.05-5.98)$	$8.02\ (5.79-11.3)\times 10^{-6}$	$0.70\ (0.59-0.84)$	$3.28\ (1.85-6.41)\times 10^{4}$	Medium
14	$4.03\ (2.21-7.06)$	$7.52\ (5.47-10.6)\times 10^{-6}$	$0.56\ (0.45-0.66)$	$3.22\ (1.90-6.19)\times 10^{4}$	Slow
16	$3.85\ (2.20-6.35)$	$7.88\ (6.04-11.6)\times 10^{-6}$	$0.46\ (0.30-0.63)$	$3.25\ (1.64-5.59)\times 10^{4}$	Slow
17	$3.60\ (2.19-5.76)$	$8.11\ (5.79-10.6)\times 10^{-6}$	$0.85\ (0.57-1.25)$	$3.28\ (1.71-5.70)\times 10^{4}$	Medium
18	$3.63\ (1.82-6.45)$	$8.07\ (6.23-11.3)\times 10^{-6}$	$0.34\ (0.26-0.38)$	$3.28\ (1.91-6.14)\times 10^{4}$	Slow
China					

C	$3.80\ (2.21-6.36)$	$7.97\ (6.12-10.5)\times 10^{-6}$	$0.77\ (0.33-1.18)$	$3.27\ (1.73-5.77)\times 10^{4}$	Medium
D	$3.91\ (2.13-6.44)$	$7.80\ (5.76-11.0)\times 10^{-6}$	$0.53\ (0.22-1.14)$	$3.19\ (1.98-6.06)\times 10^{4}$	Slow
E	$3.79\ (1.97-5.66)$	$7.98\ (6.00-11.4)\times 10^{-6}$	$0.70\ (0.35-0.97)$	$3.27(1.60-5.48)\times 10^{4}$	Medium
H	$4.52\ (2.42-5.88)$	$8.01\ (5.84-10.9)\times 10^{-6}$	$1.23\ (0.57-2.10)$	$3.22\ (2.01-5.52)\times 10^{4}$	Rapid
I	$4.08\ (2.40-6.74)$	$7.67\ (5.34-10.1)\times 10^{-6}$	$0.30\ (0.16-0.43)$	$3.25\ (1.38-5.87)\times 10^{4}$	Slow
L	$3.89\ (2.30-5.82)$	$7.82\ (5.78-10.4)\times 10^{-6}$	$0.54\ (0.21-0.94)$	$3.24\ (1.80-6.09)\times 10^{4}$	Slow
O	$5.62\ (2.70-7.00)$	$8.70\ (6.20-11.4)\times 10^{-6}$	$2.29\ (1.36-4.26)$	$3.64\ (2.18-7.07)\times 10^{4}$	Outlier
T	$3.94\ (2.38-5.96)$	$7.94\ (5.66-10.5)\times 10^{-6}$	$1.02\ (0.68-1.72)$	$3.25\ (1.77-6.08)\times 10^{4}$	Rapid

Table S3. Description of variables, parameters, and estimated parameter values: The fixed effect and random effect for each parameter were estimated by a non-linear mixed effect model and the estimates and standard errors were summarized.

Variables or parameters	Description	Unit	ϑ: Fixed effect (SE)*	Ω: SD of random effect (SE)*
$f(t)$	Relative fraction of uninfected target cells at time t to those at time 0	Unitless (fraction)	---	---
$V(t)$	Amount of virus at time *t*	RNA copies/ml	---	---
β	Rate constant for virus infection	(RNA copies/ml)$^{-1}$day^{-1}	7.95×10^{-6} (1.49×10^{-6})	0.16 (0.24)
γ	Maximum rate constant for viral replication	Day^{-1}	3.80 (1.95)	0.27 (0.28)
δ	Death rate of virus-producing cells	Day^{-1}	0.68 (0.09)	0.56 (0.09)
$V(0)$	Amount of virus at time 0 (symptom onset)	RNA copies/ml	3.27×10^{4} (1.04×10^{4})	0.32 (0.25)

* The parameter for patient k, ϑ_i $(= \vartheta \times e^{\pi_k})$ is represented as a product of ϑ (a fixed effect) and e^{π_k} (a random effect). π_k follows the normal distribution with mean 0 and standard deviation Ω.

Table S4. Sample size (per group) under different inclusion criteria

Outcome	Inhibition rate	All patients (no inclusion criteria)	Patients treated within "X days" from the onset of symptoms				
			0.5 days	1 days	2 days	3 days	4 days
Duration of virus shedding	95%	13603	249	584	1717	4556	3200
	99%	11670	166	458	1462	3837	2840
Cumulative viral load	95%	2811	12	40	209	583	915
	99%	2554	11	37	192	533	836

Reference and Notes

1. B. Cao *et al.*, A Trial of Lopinavir-Ritonavir in Adults Hospitalized with Severe Covid-19. *N Engl J Med*, (2020).
2. Y. Wang *et al.*, Remdesivir in adults with severe COVID-19: a randomised, double-blind, placebo-controlled, multicentre trial. *The Lancet*, (2020).
3. J. H. Beigel *et al.*, Remdesivir for the Treatment of Covid-19 — Preliminary Report. *New England Journal of Medicine*, (2020).
4. Z. Chen *et al.*, Efficacy of hydroxychloroquine in patients with COVID-19: results of a randomized clinical trial. *medRxiv*, 2020.2003.2022.20040758 (2020).
5. W. Tang *et al.*, Hydroxychloroquine in patients with mainly mild to moderate coronavirus disease 2019: open label, randomised controlled trial. *BMJ* **369**, m1849 (2020).
6. Y. Li *et al.*, Efficacy and Safety of Lopinavir/Ritonavir or Arbidol in Adult Patients with Mild/Moderate COVID-19: An Exploratory Randomized Controlled Trial. *Med (N Y)* **1**, 105-113.e104 (2020).
7. J. Grein *et al.*, Compassionate Use of Remdesivir for Patients with Severe Covid-19. *N Engl J Med*, (2020).
8. P. Gautret *et al.*, Hydroxychloroquine and azithromycin as a treatment of COVID-19: results of an open-label non-randomized clinical trial. *Int J Antimicrob Agents*, 105949 (2020).
9. J. Geleris *et al.*, Observational Study of Hydroxychloroquine in Hospitalized Patients with Covid-19. *N Engl J Med* **382**, 2411-2418 (2020).
10. P. Gautret *et al.*, Clinical and microbiological effect of a combination of hydroxychloroquine and azithromycin in 80 COVID-19 patients with at least a six-day follow up: A pilot observational study. *Travel Med Infect Dis* **34**, 101663 (2020).
11. H. Bian *et al.*, Meplazumab treats COVID-19 pneumonia: an open-labelled, concurrent controlled add-on clinical trial. *medRxiv*, 2020.2003.2021.20040691 (2020).